Pressure Distribution Analysis for Aerodynamic Characterization Across Varying Flight Regimes

Christian Pack[1] and Mason Roddy[2]

University of Tennessee – Knoxville, 37996

The pressure coefficient is a valuable dimensionless parameter that can be used to describe the pressure distribution along a flight vehicle's surface and estimate important aerodynamic characteristics. However, due to the diversity of conditions along varying flight regimes, special care must be taken to determine which method should be used to estimate the pressure coefficient. In this paper, several methods will be described to provide a brief introduction on how to determine a surface's pressure coefficient across supersonic and hypersonic flight regimes and evaluated. Each method will be applied to a two-dimensional tangent-ogive geometry, then analyzed against CFD results produced in Ansys Fluent and published experimental data. The critical assumptions will be discussed, and deviations of each method's accuracy will be demonstrated.

I.   Introduction

When designing high-speed flight vehicles, accurately predicting the pressure distribution is essential for estimating aerodynamic performance. As flight vehicles travel across several Mach regimes, the assumptions to the governing aerodynamic equations shift, requiring various analytical methods to estimate the pressure coefficient distribution across their surface. The pressure coefficient is a dimensionless value that allows aerodynamic performance to be determined, regardless of freestream pressure. The definition of the pressure coefficient can be seen with Eq. (1a) and a useful form is shown in Eq. (1b). This dimensionless number allows aerodynamic coefficients and forced on the body to be determined by integrating pressure coefficient or the pressure distributions over the surface, as seen in Eq. (2) and Eq. (3a) and (3b).

$$C_p \equiv \frac{P - P_\infty}{\frac{1}{2}\rho_\infty V_\infty^2} \tag{1a}$$

$$C_p = \frac{2}{\gamma M_\infty^2}\left(\frac{P}{P_\infty} - 1\right) \tag{1b}$$

$$C_l = -\oint C_p d\frac{x}{c} \tag{2}$$

$$L = -\oint p(\hat{n} \cdot \hat{y})dA \tag{3a}$$

$$D = -\oint p(\hat{n} \cdot \hat{x})dA \tag{3b}$$

---

[1] University of Tennessee – Knoxville, Undergraduate, AIAA Member.
[2] University of Tennessee – Knoxville, Undergraduate, AIAA Member.

Fluid motion in aerodynamics is largely non-linear and difficult to solve. Using the proposed methods, simple and relatively accurate estimations can be made with ease. Traditional two-dimensional analytical methods, such as Linear Supersonic Theory, Newton's Methods, Tangent-Wedge, and Shock-Expansion will be explored in this literature to gain an understanding of their application. Two-dimensional geometries will be analyzed for simplicity, however, three-dimensional corrections using the Taylor-Maccoll equations can be easily implemented, if desired. These pressure coefficient methods do not directly take viscous and other important effects into account, which can lead to some errors in specific entries. Important effects which limit the accuracy of these applications will be discussed once a better understanding of the derivations have been made. By calculating and determining the pressure coefficient with the proposed methods, engineers can optimize airfoils, fuselages, and spacecraft bodies to fit their intended design specifications without the need for complex CFD or computational power.

II.   Inclination Methods

A. Newtonian Theory

One of the earliest attempts to model and understand fluid flow was undertaken by Sir Isaac Newton using a flat plate. In his 1687 publishing of *Principia*, Newton revolutionized the world's understanding of physics and sought to explain fluid motion around a flat plate in Propositions 34 and 35 of this text. The theory is simple and follows basic Newtonian mechanics, however, this method does not model true fluid motion. His assumptions do have some accuracy at hypersonic flight, as will be shown. For the purposes of this paper, the classical derivation of Newton's Method will be neglected in favor of a modern derivation that explains the applications and simplifications made by Newton.

As mentioned previously, Newton's Method does not accurately represent fluid motion. Fluids are not merely solid particles that move in a straight line until they hit an object, transferring their momentum. Rather, they deviate from their original path to avoid incoming obstacles, (especially at low speeds). Therefore, the flow does not usually follow the assumption that the fluid moves tangentially with the surface it contacts. While Newton's assumption does not hold in most situations, it becomes more accurate as Mach number increases and can even be derived from standard compressible flow equations. To begin, the pressure coefficient definition is rearranged to a more useful derivation in Eq. (4) in which the Mach number is considered. This derivation is explained by Anderson in [1].

$$C_p = \frac{4}{\gamma + 1}\left[\sin^2\beta - \frac{1}{M_\infty^2}\right] \tag{4}$$

Taking the limit as $M \to \infty$ and the limit as $\gamma \to 1$, equation (4) becomes,

$$C_p = 2\sin^2\beta \tag{5}$$

Furthermore, these limits ($M \to \infty$ and $\gamma \to 1$) can be applied to the density ratio of a fluid across an oblique shock.

$$\frac{\rho_2}{\rho_\infty} = \frac{(\gamma + 1)M_\infty^2 \sin^2\beta}{(\gamma - 1)M_\infty^2 \sin^2\beta + 2} = \infty \tag{6}$$

Conceptually, if the density ratio goes to infinity, then the density behind the shockwave is infinitely large. To satisfy mass flow rate continuity, the shock angle, β, must equal the deflection angle, θ. This conclusion follows the $\theta - \beta - M$ relation, which is approximated for hypersonic flow Eq. (7). Applying the limit $\gamma \to 1$, the same conclusion, where $\theta = \beta$, is drawn. The full derivation can be found in [1].

$$\frac{\beta}{\theta} = \frac{\gamma + 1}{2} \tag{7}$$

With this consideration applied to Eq. (5), Newton's Method Eq. (8) can be derived. To achieve these same results. A few important assumptions and realizations were made.

$$C_p = 2\sin^2\theta \tag{8}$$

1) Newton's Method is most accurate as $M \to \infty$ and as $\gamma \to 1$, which best represents the behavior of hypersonic flow. The limit $\gamma \to 1$, is accurate for air at high speeds. Essentially, as the Mach number increases so too does the surface temperature. When at high enough temperature, chemical reactions occur and the calorically perfect assumption no longer holds as, γ, approaches one.

2) Additionally, as Mach number increases, the shock angle decreases, moving closer to the surface. This trend is illustrated in Figure 1, where the shock angle is calculated at varying Mach numbers, highlighting the previous statement that the shock angle decreases with increasing Mach numbers. As the shock angle approaches the surface, becoming almost coincident with it, Newton's original assumption that flow moves tangentially to the surface becomes a more accurate representation of reality. This is also true for blunt bodies.
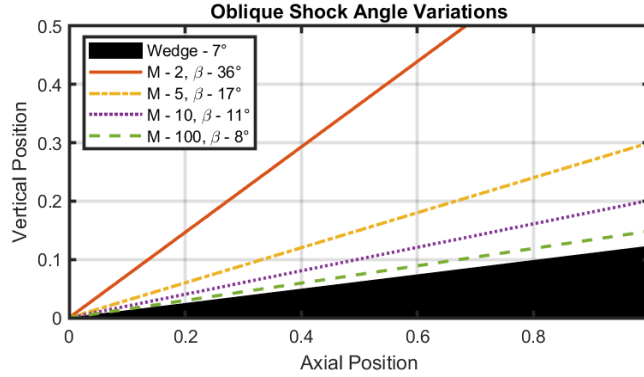
Fig. 1 Oblique Shock Angle Variations across Mach Numbers.

B. Modified Newtonian Theory

In 1955, Lester Lees introduced the Modified Newtonian Method . The purpose of this modification was to integrate Mach number dependence into the prevailing theory. This was achieved by replacing the coefficient of two in Newtonian theory with the maximum pressure coefficient at the stagnation point across a normal shock. The resulting Eq. (9) is shown below, where the pressure (and Mach number) dependence comes into play with $C_{p_{max}}$.

$$C_p = C_{p_{max}} \sin^2 \theta \tag{9}$$

$$C_{p_{max}} = \frac{P_{02} - P_\infty}{\frac{1}{2}\rho V_\infty^2} = \frac{2}{\gamma M_\infty^2}\left[\frac{P_{02}}{P_\infty} - 1\right] \tag{10}$$

The stagnation pressure ratio across a normal shock wave can be determined using the Rayleigh pitot tube formula or by using the isentropic and normal shock relations, i.e. $\frac{P_{02}}{P_\infty} = \frac{P_{01}}{P_\infty}\frac{P_{02}}{P_{01}}$.

Using the Modified Newtonian equation and the limits discussion standard Newtons Method ($M \to \infty$ and $\gamma \to 1$), $C_{p_{max}} = 2$. Simplifying Eq. (9) to Newton's Method (8). The importance of the Modified Newton's Method comes in when you realize the maximum pressure coefficient rarely reaches two across a normal shock and is usually less for a low Mach number with non-chemically reacting flow. This can be shown with Figure 2, below. It can be shown that the modified Newtonian method approaches the same Newtonian results as $\gamma \to 1$ and $M \to \infty$.
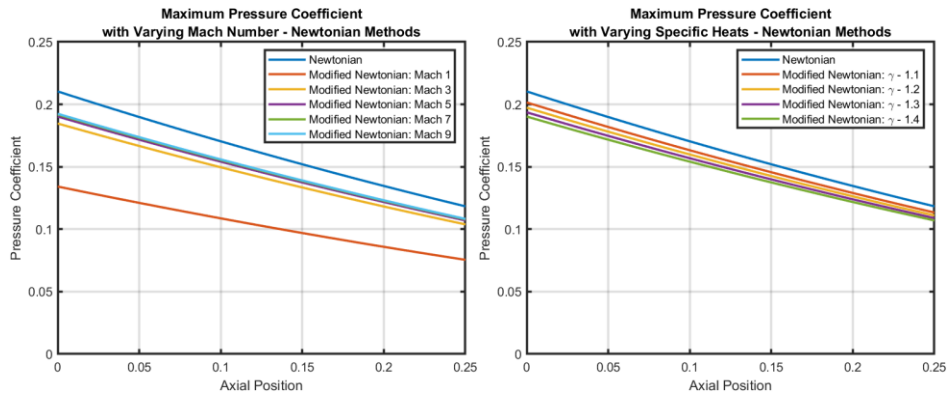
Fig. 2 Visual of the Modified Newton Method convergence to Newtonian as $M \to \infty$ and $\gamma \to 1$.

C. Tangent-Wedge Method

The Tangent-Wedge method for determining the pressure coefficient does not have exact theoretical backing. However, the estimation is simple and reasonable for a sharp, slender body with an attached shockwave, specifically, when the local inclination along the entire surface is less than the maximum turning angle at that Mach number.

The Tangent-Wedge method estimates the pressure coefficient at a local point on the surface by drawing a tangent line from the surface to the freestream, creating angle θ_i, as shown in Figure 3. This tangent line acts as a theoretical wedge, which will create an oblique shock wave. It is then assumed that the pressure on the surface of the theoretical wedge is equivalent to the pressure on the actual slender body, Eq. 11. Despite lacking theoretical derivation, this approximation provides reasonable results in hypersonic flow.

$$\frac{P_i}{P} = 1 + \frac{2\gamma}{\gamma + 1}[M_1^2 \sin^2 \beta - 1] \tag{11}$$
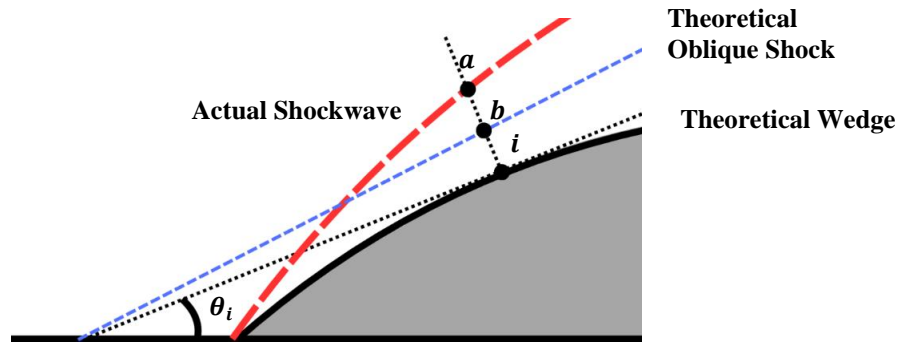
Fig. 3 Tangent-Wedge Method Diagram.

The question remains: how can this method with little theoretical support yield relatively accurate results? When flow passes through a shockwave, both its vertical and horizontal velocity components will experience a change. However, the change in the vertical component (v) is considerably smaller than the change in the horizontal component (u) for a slender body. Using Euler's equation (12), it can be implied that the pressure gradient is predominantly normal to flow direction.

$$dP = -\rho V dV \tag{12}$$

As a result, the pressure along the line, normal to the theoretical wedge at point i is relatively constant. Due to centrifugal forces, the pressure is not entirely constant along this line and is slightly higher at a than the pressure at points b and i being. The pressure behind the theoretical oblique shock wave is also slightly lower than true shock wave, making $P_b = P_i$ a relatively accurate statement.

D. Shock-Expansion Method

Similar to the Tangent-Wedge method, the Shock-Expansion method is most accurate for sharp nosed bodies with attached shock waves. Unlike the Tangent-Wedge method, this method has a more grounded theoretical backing. Here, the flow conditions are calculated across an oblique shock with the deflection equivalent to that of the nose angle, θ_n. Further down the surface, small expansions are taking place on the body. Local expansions occur between a line tangential to the surface and the freestream, θ_n, as explained in Figure 4.
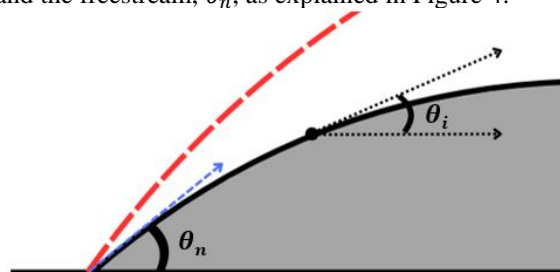
Fig. 4 Shock Expansion Method Diagram.

Using oblique shock relations, at θ_n, the post shock pressure ratio and Mach number can be calculated. With the Mach number behind the shock wave, M_n, the Prandtl-Meyer equation (13) can be used to calculate the Mach number behind the expansion at a given location, M_n.

$$\theta = \nu(M_i) - \nu(M_n) \tag{13}$$

Where the Prandtl-Meyer functions $\nu(M_i)$ and $\nu(M_n)$ can be calculated using Eq. (14).

$$\nu(M) = \sqrt{\frac{\gamma + 1}{\gamma - 1}} \tan^{-1}\left(\sqrt{\frac{\gamma - 1}{\gamma + 1}(M^2 - 1)}\right) - \tan^{-1}\left(\sqrt{M^2 - 1}\right) \tag{14}$$

Finally, combining the isentropic pressure ratios the pressure ratio between the post shock and post expansion conditions can be given as (15). Then the post expansion pressure, $\frac{P_i}{P_\infty}$, can be determined using isentropic and oblique pressure ratios, shown in Eq (16), and implemented in the definition of the pressure coefficient, Eq. (1b).

$$\frac{P_i}{P_n} = \left[\frac{1 + \frac{\gamma - 1}{2}M_n^2}{1 + \frac{\gamma - 1}{2}M_i^2}\right]^{\frac{\gamma}{\gamma - 1}} \tag{15}$$

$$\frac{P_i}{P_\infty} = \frac{P_i}{P_n}\frac{P_n}{P_{0n}}\frac{P_{0n}}{P_{01}}\frac{P_1}{P_\infty} \tag{16}$$

E.   Linear Supersonic Theory
A challenge with aircraft design is the non-linearity of the governing equations which describe how interactions occur. From this challenge came the linearization of these complex equations with small perturbation theories. As flow moves around a body, its uniform freestream condition is broken. The change in the fluid velocity around the body can be illustrated in Figure 5. Here, V_∞ represents the velocity in the freestream (assumed only in the x direction) while the vector $\boldsymbol{V}$ represent the velocity vector around the body. The prime variables represent the change in velocity in that direction, i.e. velocities u', v', and w', are the change of velocity in the x, y, and z directions.

$$\boldsymbol{V} = \begin{bmatrix} V_\infty + \boldsymbol{u'} \\ \boldsymbol{v'} \\ \boldsymbol{w'} \end{bmatrix}$$
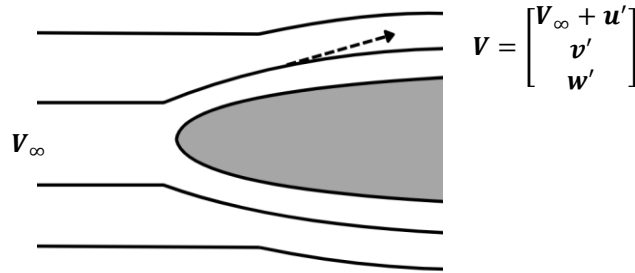
Fig. 5 Small Perturbations over a Lifting Body.

$$\nabla\boldsymbol{\Phi} = \boldsymbol{V} \tag{17}$$

$$\Phi(x, y, z) = V_\infty + \phi(x, y, x) \tag{18}$$

The above equations introduce the velocity potential. This concept will not be deeply explored in this paper; however, more information can be readily found in [3]. The velocity potential describes the velocity components of an irrotational fluid. Here, ϕ, is a newly added variable called the perturbation velocity potential. This represents the addition of the small velocity perturbations to the velocity potential. The perturbations must be small, which can be limiting, as the thickness of your body must be small. The accuracy also reduces in the transonic and hypersonic flight regimes, where perturbations and rotational flow have increased effects. With these assumptions in mind the velocity potential can be simplified to:

$$C_p = \frac{2\theta}{\sqrt{M^2 - 1}} \tag{19}$$

As previously stated, the deflection must be small due to the idea of small perturbations. Here, the assumption is that the change in velocity is negligible as the fluid moves around the body. From Figure 6, this effect can be highlighted. Using basic compressible flow equations for flow over a flat plate, the pressure coefficient calculations diverge from a deflection as small as just 4 degrees.
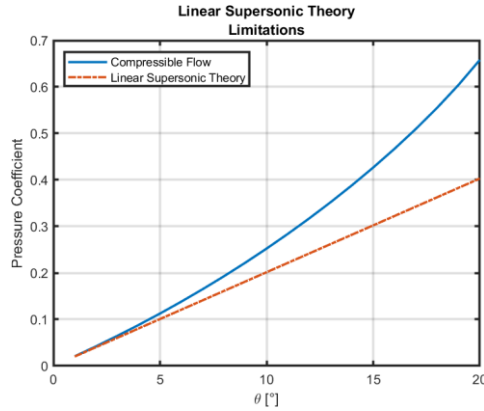
Fig. 6 Comparison of Compressible Flow and Linear Supersonic Theory with Varying Wedge Half-Angles.

III.   Computational Fluid Dynamics

F. Governing Equations and Flow Regimes

The characteristics of fluid flow are governed by the conservation laws of mass, momentum, and energy, which are mathematically described by a set of partial differential equations. These equations are fundamental to all aerodynamics and computational fluid dynamics, or CFD.

In the mid-1700s, Leonhard Euler derived the Euler equations, which describe how velocity, pressure, and density of a moving fluid are related, assuming inviscid flow ($\mu = 0$) [4].These equations combine Newton's second law applied to a fluid flow element with concepts of conservation of mass and energy. The Euler equations (Eq. 20-21) describe inviscid flow and are used in potential flow problems, simplified analytical models, or when boundary layers are not important. For example, inviscid flow is often assumed during supersonic flow when shock-wave interactions dominate the problem rather than viscosity. Regardless, Euler's equations discussed in [5] do not accurately define the shear forces, turbulence, or boundary layers of real-world aerodynamic problems.

Continuity:
$$\frac{\partial \rho}{\partial t} + \nabla \cdot (\rho \boldsymbol{V}) = 0 \tag{20}$$

$$X: \frac{\partial (\rho u)}{\partial t} + \nabla \cdot (\rho u \boldsymbol{V}) = -\frac{\partial p}{\partial x} + \rho f_x \tag{21a}$$

Momentum:
$$Y: \frac{\partial (\rho v)}{\partial t} + \nabla \cdot (\rho v \boldsymbol{V}) = -\frac{\partial p}{\partial y} + \rho f_y \tag{21b}$$

$$Z: \frac{\partial (\rho w)}{\partial t} + \nabla \cdot (\rho w \boldsymbol{V}) = -\frac{\partial p}{\partial z} + \rho f_z \tag{21c}$$

Energy:
$$\frac{\partial E}{\partial t} + \nabla \cdot [(E + p)\boldsymbol{V}] = 0 \tag{22}$$

Building on Euler's work, Claude-Lous Navier and Sir Geoge. G Stokes incorporated viscosity into the equations, resulting in the Navier-Stokes equations [6]. These equations describe how the velocity, pressure, density, temperature, and viscosity of a moving fluid are related, now incorporating viscous forces and heat conduction. These equations are applicable to both incompressible and compressible flow. For brevity, derivation is not covered in this work but can be found in [7].The compressible form of the Navier-Stokes equations is shown below.

Continuity:
$$\frac{\partial \rho}{\partial t} + \nabla \cdot (\rho \boldsymbol{V}) = 0 \tag{23}$$

$$X: \frac{\partial(\rho u)}{\partial t} + \nabla \cdot (\rho u \boldsymbol{V}) = -\frac{\partial p}{\partial x} + \rho f_x + (\nabla \cdot \tau_{xx}) \tag{24a}$$

Momentum:

$$Y: \frac{\partial(\rho v)}{\partial t} + \nabla \cdot (\rho v \boldsymbol{V}) = -\frac{\partial p}{\partial y} + \rho f_y + (\nabla \cdot \tau_{yy}) \tag{24b}$$

$$Z: \frac{\partial(\rho w)}{\partial t} + \nabla \cdot (\rho w \boldsymbol{V}) = -\frac{\partial p}{\partial z} + \rho f_z + (\nabla \cdot \tau_{zz}) \tag{24c}$$

Energy:

$$\frac{\partial E}{\partial t} + \nabla \cdot [(E + p)\boldsymbol{V}] = \nabla \cdot (k\Delta T) + \varphi \tag{25}$$

A flow is considered compressible when the density of a fluid changes significantly with pressure and typically occurs at Mach numbers greater than 0.3. This study focuses exclusively on the compressible flow across supersonic and hypersonic flight. For analytical methods, an inviscid assumption is used across all Mach regimes to simplify calculations, a common approach in aerodynamic theory. However, real-world flow will always be viscous, thus the use of the compressible Navier-Stokes equations is necessary [7]. While the Navier-Stokes equations could be solved through calculus, they are too difficult for complex cases, thus requiring computational fluid dynamics. CFD methods are used to solve these equations and accurately model boundary layers, skin friction, and viscous interactions.

G. Numerical Setup and Procedure in Ansys Fluent

Ansys Fluent can be used to solve both the Euler equations (inviscid flow) or the Navier-Stokes Equations (viscous flow), depending on the selected model. As mentioned, Euler will only be used when boundary layers are not important, often in potential flow problems [5]. All other cases in which compressible flow is present should include viscosity to better understand the boundary layer effects, drag, and heat transfer.

A tangent ogive will predominantly be used for this analysis. The tangent ogive geometry is formed by a segment of a circle that is tangent to the cylindrical body, represented in the schematic below [8]. For this study, blunt and slender ogives are compared with l/d ratios of 3 and 6 respectively.
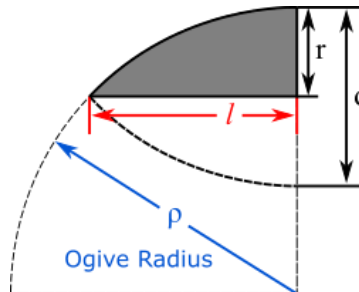
Fig. 7 Tangent Ogive Parameters.

Create an enclosed shape and define the boundaries using the "Named Selections" feature. The left, top, and right boundaries are labeled as "Farfield," representing the edges of a simulation that are far away from the object of interest. The bottom boundary and ogive boundary are defined as "symmetry" and "ogive" respectively. These named selections are used to assign boundary conditions in Fluent.
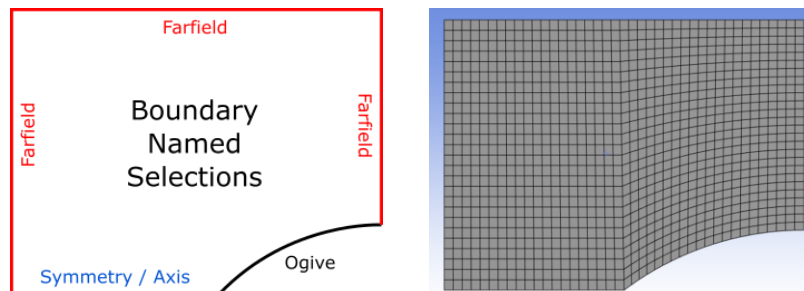
Fig. 8 Boundary "Named Selections" with Example Mesh for Ogive Simulation.

Import the geometry into Fluent and mesh the surface; refine the mesh appropriately. In the fluid settings, define the air properties of specific heat, C_p, and molecular weight, M, as 1006.43 J/kg-K and 28.966 kg/kmol respectively. Set density to "ideal gas", indicating it will be solved for using the equation of state, a requirement for compressible flow. The assumption of a constant specific heat holds for a calorically perfect gas under 1,000K [3].

As previously mentioned, all flow types will be evaluated using compressible flow and viscous flow assumptions, with the default k-omega Shear Stress Transport (SST) model. For supersonic and hypersonic flows where shock interactions dominate, the Reynolds Stress Model (RSM) is recommended to better predict turbulent behavior.

The ogive boundary condition is set to "wall." For 2D analysis, set the boundary condition on the bottom boundary to "symmetry", and for 3D, set it to "axis" with the solver set to "axisymmetric." This will be useful when comparing the numerical results to experimental data. Finally, set the Farfield boundary condition to "pressure-far-field." The gauge pressure is set to P_g = 101,325 Pa, the operating conditions pressure is set to P_0 = 0 Pa, and temperature T = 300 K, which models standard atmospheric conditions at sea level. The input parameters are summarized in Table 1.

Table 1. Ansys Input Parameters or Settings for all Flight Regimes

Parameter	Value	Parameter	Value
Solver Type	Density-based	Air: Specific Heat (C_p)	1006.43 J/kg-K
Viscous Model	k-omega SST (default) RSM (super/hypersonic)	Air: Molecular Weight (M)	28.966 kg/kmol
Solver Type	Wall	Air: Density	Ideal Gas Law
Ogive BC	Wall	Farfield: Operating Pressure (P_0)	0 Pa
Farfield BC	Pressure-far-field	Farfield: Gauge Pressure (P_g)	101325 Pa
Symmetry BC / Space Solver	2D: Symmetry / Planar 3D: Axis / Axisymmetric	Farfield: Temperature (T)	

IV.   Results and Discussion

H. CFD and Analytical Validation

For validation of the simulation's parameters, the models were compared with experimental results found in Anderson [1]. This was conducted on a three-dimensional tangent ogive. This study uses an ogive with a l/d ratio of 3 and is tested at Mach 2.73 and 5.05. Additionally, the analytical methods discussed previously were adapted to represent a three-dimensional case, meaning the solvers used the Taylor-Maccoll equations, when necessary, and the ogive was computed as an axisymmetric body in ANSYS. The pressure coefficient for experimental, analytical, and simulation data are shown in Figure 9.
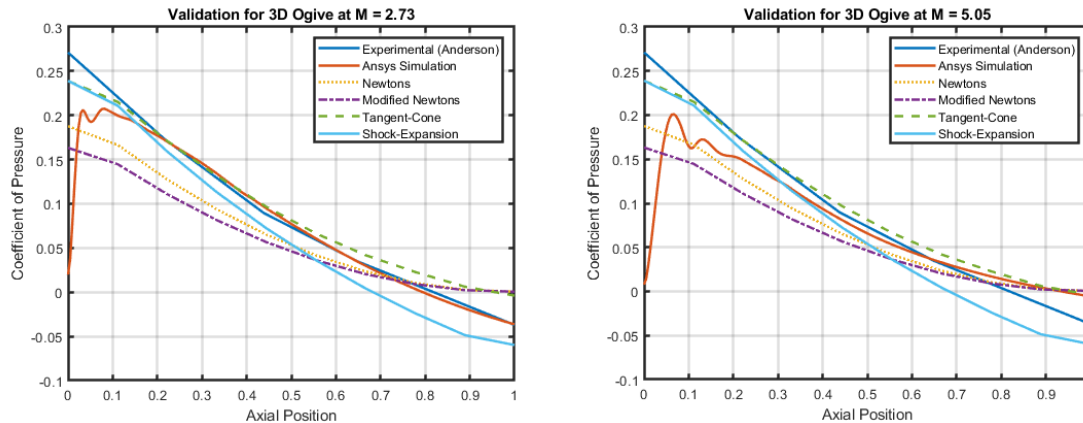
Fig. 9 Validation Results comparing Experimental, Ansys Simulation, and Analytical Methods.

As shown above, the solvers accurately follow the experimental data. So, to do the analytical models (other than the Newtonian methods). This is expected, as these are most accurate in high speed slow for blunt bodies.

I. Results

A comparison of each of these results is shown in Figure 10. Here, the CFD results are generally viewed as the most accurate model. In these figures, a two-dimensional tangent ogive with an l/d ratio of 3 was used. Four cases are shown of varying Mach numbers (1.5, 3, 5, and 7) to understand the trends of this data.
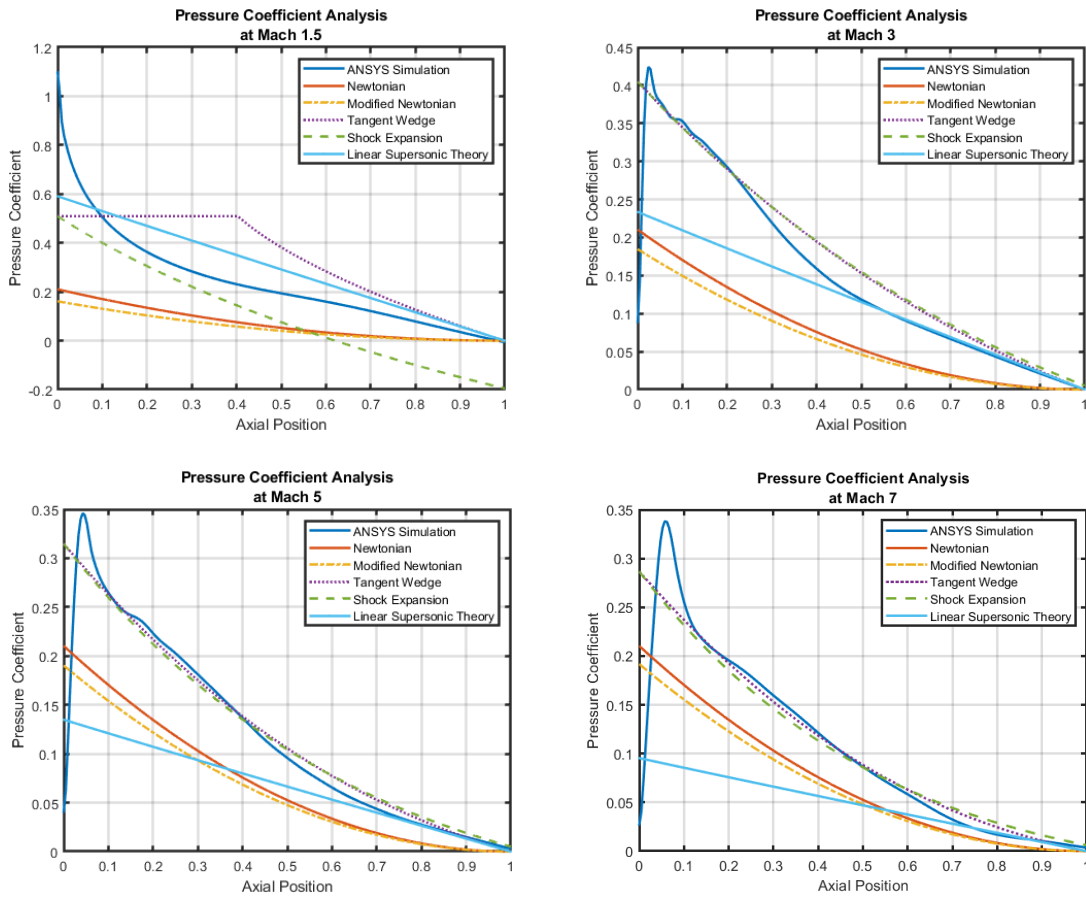
Fig. 9 Pressure Coefficient calculated for an ogive (l/d = 3) at Mach numbers 1.5, 3, 5, and 7.

In the supersonic, Mach 1.5 case, the Newtonian methods underrepresent the expected pressure coefficient (CFD results). So too does the Shock Expansion method, this is likely due to the fact that at these relatively low Mach numbers, reflected shocks interfere with the surface. This effect is not considered with this method and leads to error (further explanation in next section). The trends shown in the latter two cases are as expected. The Newtonian methods once again undervalue the pressure coefficient; however, the true accuracy of these methods lie at very high speeds and blunt bodies, which the other methods could not accurately solve. The CFD generally follows the Tangent-Wedge and Shock Expansion methods (especially at high Mach numbers), which shows good correlation to one another. One interesting trend to acknowledge is the increased accuracy of linear supersonic theory downstream of the body. This could be due to the fact that the local inclination decreases to an angle which yields accurate results. This trend is not followed in the Mach 7 case, likely due to the increase of rotational flow effects. A sharp spike in the CFD data for all of these cases is likely due to viscous effects, explained below.

All of these methods are compared across a range of Mach numbers from Mach 1 to Mach 10 in Figure 11. Here, these methods were used to calculate the average pressure coefficient along the body of an ogive at several Mach numbers. These results show general trends across a wider Mach range. The CFD follows the Tangent-Wedge and Shock expansion methods fairly well, while the linear supersonic theory loses accuracy with Mach number. Around Mach 5 the Newtonian theories start to show better results and create an accurate representation of the fluid characteristics.
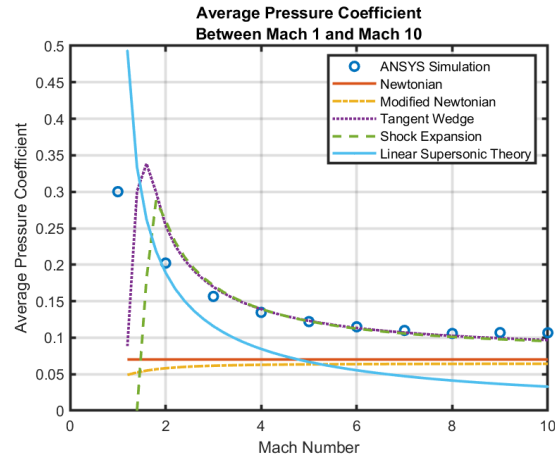
Fig. 101 Comparison of Analytical and Simulation Pressure Coefficients for an ogive with l/d = 3.

J. Limiting Effects

There are several factors which contribute to the variation seen between the analytical methods presented and the CFD results. These effects are highlighted below and in Figure 12 as well.

1) *Viscous interactions* – At high Mach numbers a large amount of kinetic energy is transferred to the fluid which increases its temperature (viscous dissipation) and viscosity, creating a thick boundary layer near the surface. The viscous boundary layer grows with Mach number, which pushes the inviscid region farther from the surface. The two boundary layers interact, leading to "viscous interactions". This leads to significant increases in the local pressure distribution; thus, the pressure can be underrepresented if this interaction is not considered. The CFD takes these into consideration while the analytical models do not. Which explains the sharp increase in at the leading edge.

2) *Rotational flow* – A critical assumption for the velocity potential question, thus linear supersonic theory, is that the flow is irrotational (vorticity is zero). In subsonic and supersonic flow this is an accurate assumption. However, in hypersonic and transonic flight, rotational flow is common. For hypersonic flight, this is due to the viscous boundary layer and the curved shockwaves it creates. Thes curved shockwaves also produce rotational flow. Because of this effect, linear supersonic theory loses accuracy around the Hypersonic regime.

3) *High temperature effects* – As temperature increases, so too do the chances of chemical reaction. Chemical reactions break the assumption of a calorically perfect gas (constant specific heat), which is the backbone of basic compressible flow equations. Thus, methods taking this effect into consideration must be implemented. As stated previously, Newton's method experiences more accuracy in this situation. The CFD simulation in ANSYS does not include these effects, as γ is constant, and loses some accuracy with Mach number.

4) *Reflected Shock Waves* – After shockwaves form, they can move downstream and reflect off of surfaces. When the flow is expanding small Mach waves form from the expansion. These can reflect off of the initial shock wave, hit the body, and interfere with the surface pressure. This phenomenon is more critical at low sonic speeds where the reflected shock waves have a higher chance of being reflected onto the body, due to the shape of the initial shock wave.

5) *Three-dimensional relief* – With a two-dimensional wedge, the mass flow rate is set by the shock wave and their streamlines are constant. With a three-dimensional cone, the mass flow rate is set by the shockwave, but the streamlines have room to disperse and reduce the intensity of the shockwave. This effect is the reason a conical shock solver (Taylor-Maccoll) must be used to analyze the tangent ogive in three-dimensions.
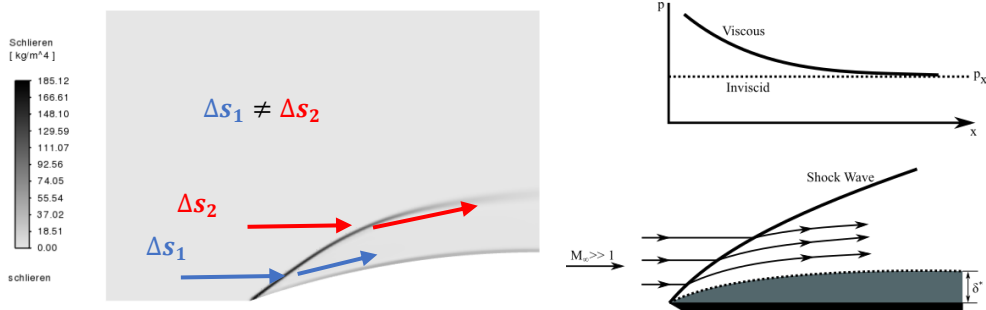
Fig. 112 Visuals of limiting effects, (Left) Curved shock waves, (Right) Viscous interactions.

V.   Conclusion

Through this paper, several analytical methods were derived to explore pressure coefficient determination across a body. Table 2 summaries these methods and their assumptions. These results were then compared to CFD and some experimental data. Critical effects and limitations are highlighted and discussed in the previous section.

Table 2. Review of Methods and Assumptions

Method	Equation	Assumptions
Newtonian Methods	$$C_p = 2\sin^2\theta$$ *or* $$C_p = C_{p_{max}}\sin^2\theta$$	Flow is tangent to the surface: $M \to \infty$ and $\gamma \to 1$ Also good for blunt bodies
Tangent Wedge	$$C_p = \frac{2}{\gamma M_\infty^2}\left(\frac{P_i}{P_\infty} - 1\right)$$ where P_i is the local pressure behind an oblique shockwave	Slender bodies with attached shockwaves
Shock Expansion	$$C_p = \frac{2}{\gamma M_\infty^2}\left(\frac{P_i}{P_\infty} - 1\right)$$ where P_i is the local pressure behind an oblique and expansion wave	Slender bodies with attached shockwaves
Linear Supersonic	$$C_p = \frac{2\theta}{\sqrt{M^2 - 1}}$$	Irrotational and isentropic flow with small perturbations (thin bodies)

References

[1]   J. D. Anderson Jr., Hypersonic and High-Temperature Gas Dynamics, Fourth Edition (AIAA Education), 2019.

[2]   L. Lees, "Hypersonic Flow," *Journal of Spacecraft and Rockets,* pp. 241-276, 1955.

[3]   J. D. Anderson Jr., Modern Compressible Flow With Historical Perspective, Fourth Edition, McGraw-Hill, 2021.

[4]   National Aeronautics and Space Administration, "Euler Equations," 2021.

[5]   F. White and H. Xue, Fluid Mechanics, 2021.

[6]   National Aeronautics and Space Administration, "Navier-Stokes Equations," 2021.

[7]   J. D. Anderson Jr., Fundamentals of Aerodynamics, 2023.

[8]   G. A. C. Sr., "The Descriptive Geometries of Nose Cones," 1996.

[9]   C. Simulations, "Physics Setup, Supersonic Flow Over a Wedge," 2024.

[10] R. M. C. John J. Bertin, Aerodynamics for Engineers, Sixth Edition, Cambridge University Press, 2022.